THE ASTROPHYSICAL JOURNAL, 342:928–933, 1989 July 15

THE NONLINEAR TRANSFER PROBLEM IN ACCRETING PULSARS: STIMULATED SCATTERING EFFECTS

S. G. ALEXANDER AND P. MÉSZÁROS
Pennsylvania State University
AND
R. W. BUSSARD
University of Arizona and NASA Marshall Space Flight Center
Received 1988 October 17; accepted 1988 December 30

ABSTRACT

We solve the accreting pulsar radiative transfer problem in the presence of nonlinear effects in the radiation field, in particular those introduced by stimulated scattering. This leads to an extension of the Feautrier method in the strong magnetic case, which is solved by iterations. We also introduce relativistic cross sections and compare their effect to the nonrelativistic approximation. This affects the cyclotron line shape and energy. We find that stimulated scattering is important in determining the flux level in the continuum above the effective thermalization frequency and also in determining the cyclotron line flux.
Subject headings: pulsars — radiation mechanisms — radiative transfer — stars: accretion

I. INTRODUCTION

The X-ray emission region of accreting magnetized neutron stars is determined by a number of processes, several of which can depend on the radiation field in a nonlinear way. Among these are the induced Compton scattering, two-photon scattering, and resonance effects associated with the non–LTE population of Landau levels. For the most part, the nonlinearity in these effects has been neglected (e.g., Ventura, Nagel, and Mészáros 1979; Nagel 1981*a*, *b*; Kaminker, Pavlov, and Shibanov 1982, 1983; Mészáros and Nagel 1985*a*, *b*, and references therein), mainly in order to simplify the problem to a manageable level. This simplification is adequate to a certain degree in many but not all situations. Thus, in the level population problem it is approximately justifiable if the cyclotron ground energy is much higher than the typical temperature, $\hbar\omega_c \gg kT$ (see Bussard 1980). The stimulated Compton effect nonlinearity is most important at low photon energies, $\hbar\omega \ll kT$, this being one of the effects that drives the spectrum toward the Planck equilibrium value. Typically, this effect becomes apparent in accreting pulsars at energies below several keV, and most transfer calculations have either ignored this energy region or else have ensured an approach to the Planck value at low energies with the use of stimulated emission, which can be included in a linear way; this is largely justified by the fact that at these low energies absorption starts dominating over scattering (Harding *et al.* 1984). In two-photon scattering, calculations so far (Bussard, Alexander, and Mészáros 1986; Kirk and Melrose 1986) have estimated the nonlinear contribution of the radiation field assuming it was near equilibrium value. However, a complete study of this problem requires a full treatment of the nonlinearities. It also requires a consideration of special relativistic effects in the scattering, since these can be equally important (Bussard, Alexander, and Mészáros 1986; Daugherty and Harding 1987). This is especially true for understanding and modeling correctly the cyclotron line profiles when the radiation field is not at the equilibrium value, and if one wants to study higher cyclotron harmonics, for which the non–LTE level population needs to be known. The simplest nonlinear problem, however, is that posed by the induced Compton scattering, which contributes to forming the Rayleigh-Jeans portion of the spectrum and also contributes significantly in determining the intensity of the cyclotron line, this being caused mainly by resonant scattering.

In this paper we discuss a treatment of the nonlinear effects in magnetized scattering atmospheres, which is an extension of the Feautrier method. This treatment is applied in particular to the problem of stimulated Compton scattering in strongly magnetized ($\hbar\omega_c \gg kT$) accreting pulsars. The formalism can be extended to include the other effects mentioned above, which should make it also useful in modeling gamma-ray bursters. In § II we discuss the treatment of the nonlinearities in the transfer problem and outline the numerical method. Calculations with parameters typical of X-ray pulsars under various assumptions are presented in § III, using both nonrelativistic and relativistic cross sections. The results are discussed in § IV and are compared with previous nonlinear calculations by Nagel (1982) and with the approximate treatment by Mészáros, Pavlov, and Shibanov (1989). The applicability of such calculations for realistic accreting neutron star atmospheres is considered, as well as their usefulness for comparison with observations of X-ray pulsars and gamma-ray bursters.

II. TRANSFER EQUATION WITH STIMULATED PROCESSES

The radiative transfer equation for plane-parallel, or slab, geometry for photon occupation number, N_α, where α labels the photon frequency, ω, solid angle, Ω, and polarization, m, can be expressed as

$$\mu \frac{dN_\alpha}{dz} = -\kappa_\alpha N_\alpha + Q_\alpha . \tag{1}$$

In equation (1), $\mu = \cos\theta$, where θ is measured from the normal to the slab, and κ_α and Q_α are the total opacity and source, respectively. Including stimulated processes, these are

$$\kappa_\alpha = \sum_{\alpha'} e^{(\omega-\omega')/T} R_{\alpha\alpha'}(1 + N_{\alpha'}) + \kappa_\alpha^{\rm ff} , \tag{2}$$

$$Q_\alpha = \sum_{\alpha'} R_{\alpha\alpha'} N_{\alpha'}(1 + N_\alpha) + \kappa_\alpha^{\rm ff} N_{\rm BB} , \tag{3}$$

where the first term in each equation accounts for scattering and the second term for free-free absorption and emission, and the summation over α' is shorthand for the summation over polarization and integration over frequency and solid angle. The redistribution function for scattering from photon (ω, Ω, m) to photon (ω', Ω', m') in terms of the differential cross section is

$$R_{\alpha\alpha'} \equiv e^{(\omega'-\omega)/T} \frac{d^2\sigma}{d\omega' d\Omega'} (\omega, \Omega, m \rightarrow \omega', \Omega', m') , \qquad (4)$$

where the condition of detailed balance has already been used in equation (3). The stimulated processes are contained in the $(1 + N_\alpha)$ factors and the use of the Planck, or blackbody, occupation number, $N_{\rm BB} = (e^{\omega/T} - 1)^{-1}$, in the free-free emission.

We follow here the complete linearization method as in Mihalas (1978). First, the second-order transfer equation for photon density variable $U_\alpha \equiv \frac{1}{2}[N_\alpha(+\mu) + N_\alpha(-\mu)]$ is

$$\frac{\mu^2}{\kappa_\alpha} \frac{d}{dz}\left(\frac{1}{\kappa_\alpha}\frac{dU_\alpha}{dz}\right) = U_\alpha - \frac{Q_\alpha}{\kappa_\alpha} . \qquad (5)$$

Next, assume that all quantities in equation (5) can be represented by a known value plus a small perturbation; e.g., $U_\alpha = U_\alpha^0 + \delta U_\alpha$, etc. After expanding equation (5) and keeping only terms linear in any δ-quantities, we obtain

$$L_\alpha = \frac{\mu^2}{\kappa_\alpha^0}\left[-\frac{d}{dz}\left(\frac{1}{\kappa_\alpha^0}\frac{d\delta U_\alpha}{dz}\right) + \frac{\delta\kappa_\alpha}{\kappa_\alpha^0}\frac{d}{dz}\left(\frac{1}{\kappa_\alpha^0}\frac{dU_\alpha^0}{dz}\right) + \frac{d}{dz}\left(\frac{\delta\kappa_\alpha}{\kappa_\alpha^{02}}\frac{dU_\alpha^0}{dz}\right)\right] + \delta U_\alpha - \frac{\delta Q_\alpha}{\kappa_\alpha^0} + \frac{\delta\kappa_\alpha}{\kappa_\alpha^{02}} Q_\alpha^0 , \qquad (6)$$

where L_α is the zeroth-order operator defined by

$$L_\alpha \equiv \frac{\mu^2}{\kappa_\alpha^0}\frac{d}{dz}\left(\frac{1}{\kappa_\alpha^0}\frac{dU_\alpha^0}{dz}\right) - U_\alpha^0 + \frac{Q_\alpha^0}{\kappa_\alpha^0} . \qquad (7)$$

If $\delta\kappa_\alpha$ and δQ_α depend linearly on δU_α, then equation (6) is a linear equation for δU_α that can be solved by the standard Feautrier method (see Mihalas 1978). The details of casting equation (6) in the discrete finite-difference Feautrier form with the proper boundary conditions are contained in the Appendix.

It remains to write out the explicit forms of κ_α^0, Q_α^0, $\delta\kappa_\alpha$, and δQ_α in equation (6). First, the source term for scattering in equation (3) is split into two parts. The first part in the summation is just the normal in-scattering source without stimulated processes, $R_{\alpha\alpha'} U_{\alpha'}$, while the remaining part, $R_{\alpha\alpha'} U_{\alpha'} U_\alpha$, can be treated as a negative opacity in the transfer equation. So after linearizing the total source and opacity are

$$Q_\alpha^0 = \sum_{\alpha'} R_{\alpha\alpha'} U_{\alpha'}^0 + \kappa_\alpha^{\rm ff} N_{\rm BB} , \qquad (8)$$

$$\kappa_\alpha^0 = \sum_{\alpha'} R_{\alpha\alpha'}[e^{(\omega-\omega')/T}(1 + U_{\alpha'}^0) - U_{\alpha'}^0] + \kappa_\alpha^{\rm ff} , \qquad (9)$$

and,

$$\delta Q_\alpha = \sum_{\alpha'} R_{\alpha\alpha'} \delta U_{\alpha'} , \qquad (10)$$

$$\delta\kappa_\alpha = \sum_{\alpha'} R_{\alpha\alpha'}[e^{(\omega-\omega')/T} - 1]\delta U_{\alpha'} . \qquad (11)$$

So given a starting radiation field, U_α^0, the solution of equation (6) for δU_α can be iterated until convergence.

III. RESULTS

Detailed calculations of the radiation spectra emitted from an accreting compact object have been presented by Mészáros and Nagel (1985*a*, *b*). Their self-emitting model contains nonrelativistic Compton scattering and free-free effects; however, stimulated scattering is not included. Nagel (1982) presents a solution of the full nonlinear problem using nonrelativistic cross sections, but the details of his method are not included. The effects of stimulated scattering in X-ray sources have most recently been discussed by Mészáros, Pavlov, and Shibanov (1989). In this work, an artificial detailed balance condition is used to relate the in-scattering and the out-scattering terms. This condition replaces the exponential in equation (4) by the factor $(e^{\omega'/T} - 1)/(e^{\omega/T} - 1)$ and gives the correct saturated spectrum at low energies.

Here we will solve the full nonlinear problem by the iteration procedure outlined in § II using the relativistic Compton scattering cross sections as given in Bussard, Alexander, and Mészáros (1986). To compare with the nonrelativistic case, these cross sections are calculated in the lowest order only up to the first cyclotron harmonic. Free-free emission and absorption are the same as that of Mészáros and Nagel (1985*a*, *b*), and vacuum polarization effects are included. All of the runs presented below use a grid of 32 frequencies and one angle for two polarization modes.

It was found that convergence can be attained throughout the radiation field if the starting solution is the blackbody or Planck function. In addition, a convergence damping term is included to keep the corrections within the assumed small perturbation limit. Figure 1 shows the emitted flux of photons from the slab for each iteration for a run that is discussed below (see Fig. 3). The solution converges very quickly in the continuum, while several more iterations are required to define the absorption line.

Calculations were made that duplicate the conditions of Nagel (1982): cyclotron energy, $\hbar\omega_c = 50$ keV; density, $\rho = 1.0$ g cm^{-3}; temperature, $kT = 10$ keV; and slab thickness, $R = 1 \times 10^5$ cm (semi-infinite atmosphere). Figure 2 gives the emitted photon flux for nonrelativistic scattering, and the final converged solution (curve C) is identical to Nagel's solution. Figure 3 is the corresponding solution in the relativistic case. In both graphs the calculated flux is shown for (A) no stimulating scattering, (B) the artificial detailed balance condition of

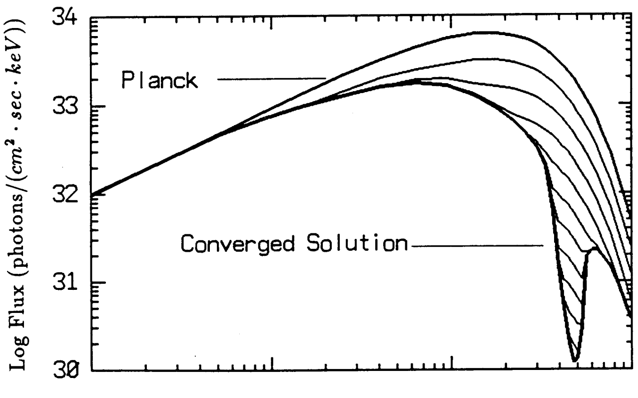

FIG. 1.—Flux spectrum for each iteration with slab parameters as in Fig. 3.

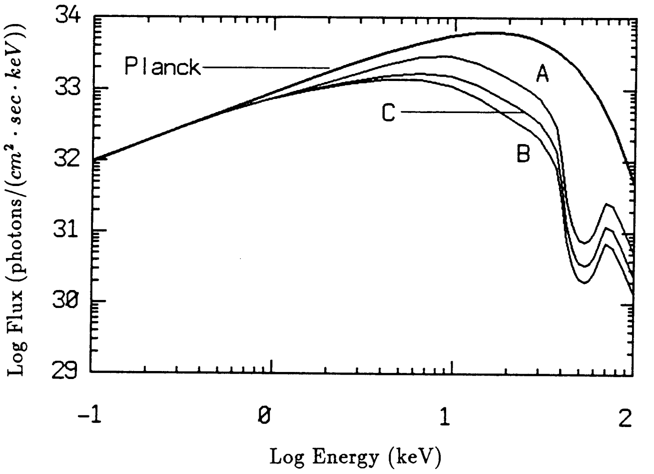

FIG. 2.—Flux spectra using nonrelativistic cross sections: (A) no stimulated scattering; (B) artificial detailed balance approximation; (C) iteration solution of nonlinear equation.

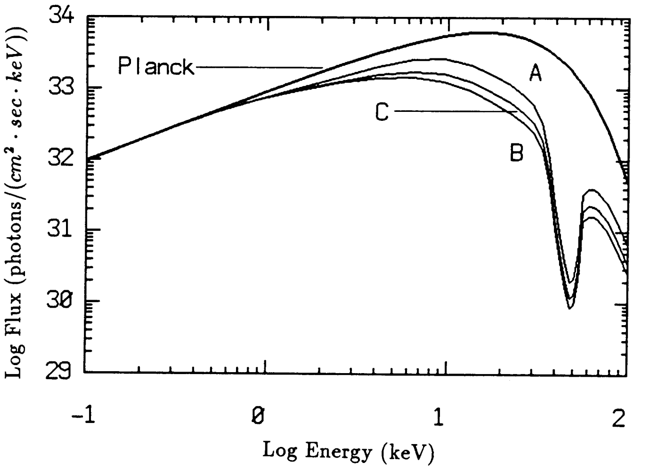

FIG. 3.—Flux spectra using relativistic cross sections: (A) no stimulated scattering; (B) artificial detailed balance approximation; (C) iteration solution of nonlinear equation.

Mészáros, Pavlov, and Shibanov (1989), and (C) the iteration procedure described here. It is seen that all cases saturate to the Planck spectrum at low energies. This is due to the stimulated free-free emission that dominates over the scattering at these energies. In either the nonrelativistic or the relativistic case, neglecting the stimulated scattering above a few keV causes a large excess of photons in both the continuum and the line. For this slab thickness, this leads to an error in the luminosity of a factor greater than 2. On the other hand, it appears that the artificial detailed balance approximation (B) overestimates the effects of stimulated scattering.

Comparing the spectra produced by the nonrelativistic and the relativistic cross sections, one sees general agreement below ~ 30 keV; however, in the region of the cyclotron line there are differences. The relativistic spectra show a much faster dropoff in the red wing with a deeper absorption line and a steeper blue wing. In addition, the location of the line is at a slightly lower energy in the relativistic case.

Stimulated scattering will be important when the $1 + N_\alpha$ factors in equations (2) and (3) are sufficiently different from unity to affect the opacity and source. One place this occurs is at low photon energies where there is thermal saturation; however, as we have seen above, this range is dominated by free-free absorption and emission which will determine the low-energy end of the spectrum.

The $1 + N_\alpha$ factor can also have a large effect in a thick slab where photons will suffer many scatterings before escaping. Figure 4 shows a set of runs for slabs with varying thickness. Here the parameters of the plasma are $\hbar\omega_c = 38$ keV; $\rho = 0.5$ g cm^{-3}; and $kT = 10$ keV; relativistic cross sections are used throughout. Run A is for a thickness of 1×10^5 cm ($\sim 2 \times 10^4$ Thomson depths, τ_T), which is essentially a semi-infinite slab. Here the effect of stimulated scattering is the largest. At a considerably smaller thickness of 50 cm ($\tau_T \sim 10$), run B shows that stimulated scattering still affects the spectrum throughout the continuum and the line. Finally, run C for a thickness of 10 cm ($\tau_T \sim 2$) shows just marginal effects, while run D for 0.1 cm ($\tau_T \sim 0.02$) is completely unaffected by stimulated scattering.

The value of the plasma density has several effects on the emitted photon flux spectrum. This is shown in Figure 5 where

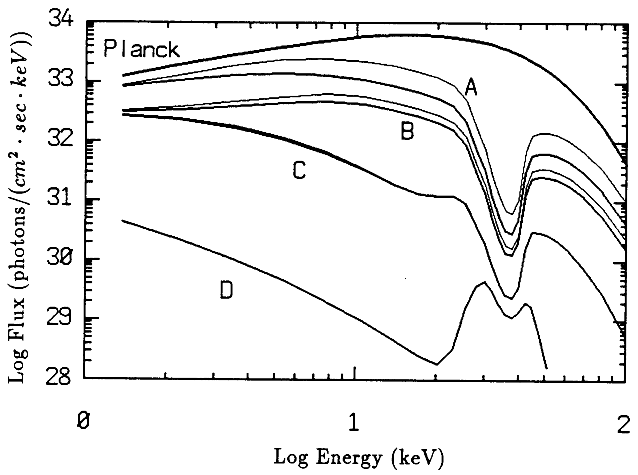

FIG. 4.—Flux spectra for various slab thicknesses: (A) 1×10^5 cm ($\tau_T \sim 2 \times 10^4$); (B) 50 cm ($\tau_T \sim 10$); (C) 10 cm ($\tau_T \sim 2$); (D) 0.1 cm ($\tau_T \sim 0.02$). For each the light line is the case for no stimulated scattering, while the dark line includes stimulated scattering.

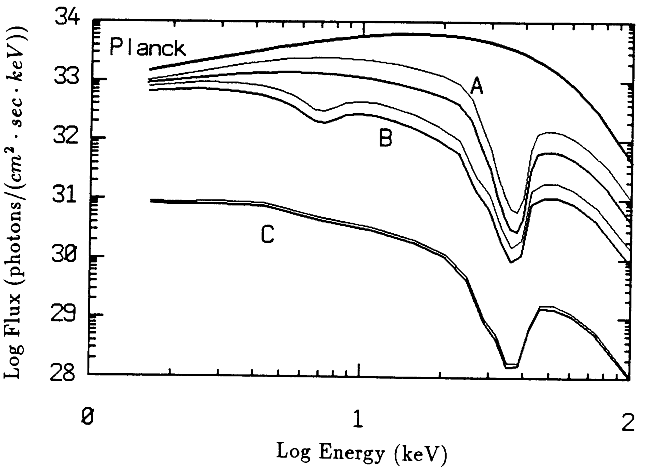

FIG. 5.—Flux spectra for a fixed slab thickness, 1×10^5 cm, for various plasma densities: (A) $\rho = 0.5$ g cm^{-3} ($\tau_T \sim 2 \times 10^4$); (B) $\rho = 5 \times 10^{-2}$ g cm^{-3} ($\tau_T \sim 2 \times 10^3$); (C) $\rho = 1 \times 10^{-3}$ g cm^{-3} ($\tau_T \sim 40$). For each the light line is the case for no stimulated scattering, while the dark line includes stimulated scattering.

the results for runs with different densities are plotted. All of these calculations are for a fixed slab thickness of 1×10^5 cm, $\hbar\omega_c = 38$ keV, $kT = 10$ keV, and three values of the density: (A) $\rho = 0.5$ g cm^{-3} ($\tau_T \sim 2 \times 10^4$) (same as run A in Fig. 4); (B) $\rho = 5 \times 10^{-2}$ g cm^{-3} ($\tau_T \sim 2 \times 10^3$); and (C) $\rho = 1 \times 10^{-3}$ g cm^{-3} ($\tau_T \sim 40$). As compared to Figure 4, for smaller densities the luminosities for similar optical depths are considerably lower here. This is because the only source of photons is free-free emission that depends quadratically on the electron density. Another effect that becomes more apparent at lower densities is vacuum polarization, i.e., the interaction of the photons with the virtual electron positron pairs in the vacuum (Ventura, Nagel, and Mészáros 1979). The cross sections are vacuum dominated between the two vacuum frequencies, $\hbar\omega_{v1} \sim 3(n_e/10^{22}\ \mathrm{cm}^{-3})^{1/2}(B/4.414 \times 10^{12}\ \mathrm{G})^{-1}$ keV and $\hbar\omega_{v2} \sim \hbar\omega_c$ (Mészáros and Ventura 1978, 1979; Gnedin, Pavlov, and Shibanov 1978; Pavlov and Shibanov 1979). Thus, in Figure 5, the continuum flux below the resonance in run A is plasma dominated, while that of run C is vacuum dominated. For run B, $\hbar\omega_{v1} \sim 7$ keV, so run B shows plasma-dominated modes below $\hbar\omega_{v1}$, and vacuum-dominated modes between $\hbar\omega_{v1}$ and the cyclotron frequency. The vacuum "dip" that is expected in a homogeneous atmosphere is seen in run B around $\hbar\omega \sim 7$ keV. The effects of stimulated scattering are seen to be very similar to those shown in Figure 4 where the effect varies inversely with the Thomson optical depth.

IV. DISCUSSION

A technique has been presented that permits the inclusion of the nonlinear stimulated scattering terms in the radiative transfer equation. This iterative procedure allows the continued use of the standard Feautrier procedure, and here this has been specialized to the case of polarized transfer in a strongly magnetized neutron star atmosphere. In addition, this technique is general enough to handle other nonlinear processes, such as the non–LTE population problem and the two-photon scattering in a magnetic field (see Bussard, Alexander, and Mészáros 1986), a treatment of which will be presented separately (Alexander, Mészáros, and Bussard 1989).

The effects of stimulated scattering have been examined in models of accreting pulsars using both nonrelativistic and relativistic cross sections. Both of these effects contribute in a different manner to determining the cyclotron line profile. While the nonrelativistic and relativistic calculations show good agreement in the low-energy continuum, differences in the line location and shape are apparent. The relativistic line trough is at slightly lower energies and is sharper than the corresponding nonrelativistic trough for the same atmosphere conditions. This difference is due to the resonant denominators in the cross sections (e.g. Pavlov, Shibanov, and Yakovlev 1980; Bussard, Alexander, and Mészáros 1986), which, even for relatively low temperature such as 10 keV, can produce noticeable differences in the escaping spectrum. We note that the shape of the absorption fits to the cyclotron line in Her X-1 (Voges *et al.* 1982) resemble our relativistic profiles of Figures 1 and 3 more than the nonrelativistic profiles of Figure 2, especially in what concerns the depth and sharpness of the feature and of the blue wing shoulder.

The convergence in this iteration method is achieved smoothly, typically in less than 15 to 20 iterations. The method therefore is stable and gives reproducible results. We tested this by reproducing the test results obtained by Nagel (1982) for the nonrelativistic stimulated scattering, using a different code. A comparison can also be made with the much faster simplified treatment of stimulated scattering of Mészáros, Pavlov, and Shibanov (1988), which uses the linear equations and approximates the effect of stimulated scattering by using an artificial detailed balance in the spontaneous scattering terms. While these methods correctly reproduce the Rayleigh-Jeans behavior at low energies, for the parameters used here this is mainly caused by the free-free absorption and stimulated emission. At energies above those where the stimulated scattering starts to be important, the artificial detailed balance and the iteration method produce essentially similar results for a while but start giving different results before the thermal turnover of the spectrum is reached. The artificial detailed balance spectrum runs parallel and closer to the correct nonlinear spectrum than it does to the spectrum neglecting stimulated scattering. The usefulnesss of this method is that it does not involve iterations and yields the Planck limit even in the absence of absorption. However, the artificial detailed balance tends to exaggerate the stimulated scattering effects, being based as it is on replacing the $1 + N_\alpha$ factor with its equilibrium value. Thus, the deeper one is in the atmosphere or the closer the spectrum is to blackbody, the closer are the artificial detailed balance results to the exact nonlinear results.

In general, the effect of stimulated scattering is to reduce the line flux with respect to the value obtained using spontaneous scattering alone, and this is true also of the continuum below the line. However, the effective spectral slope of the spectrum remains essentially the same as in the case of spontaneous scattering alone, since the cross sections are the same. The stimulated scattering spectral effects are unimportant for low optical depths, but for scattering optical depths greater than several Thomson units they start becoming important. For $\tau_T \gtrsim 10$, the differences are of the order of 50% or greater in the flux. This indicates that this phenomenon is important in interpreting and fitting X-ray pulsar spectra, but it may not be necessary in considerations of gamma-ray burster models, which appear to have $\tau_T \lesssim$ few. In the latter, however, and also in accreting pulsars and in any high-temperature magnetized objects with $T \gtrsim 10$ keV, the inclusion of relativistic effects in the cross sections is important for an accurate spectral fit.

This research has been supported in part through NSF grant AST 85-14735 and NASA grant NAGW-1522.

APPENDIX

Equation (6) in § II can be cast in discrete finite-difference form so that a standard set of Feautrier equations may be solved. For α representing a discrete set of frequencies, angles, and two polarization modes, we have the linear relations

$$\delta\kappa_\alpha = \sum_{\alpha'} E_{\alpha\alpha'}\,\delta U_{\alpha'}\ , \tag{A1}$$

$$\delta Q_\alpha = \sum_{\alpha'} F_{\alpha\alpha'}\,\delta U_{\alpha'}\ . \tag{A2}$$

In general, $E_{\alpha\alpha'}$ and $F_{\alpha\alpha'}$ may be depth dependent. This is not the case for stimulated scattering in a homogeneous plasma; however, in what follows, this dependence will be included. The slab is divided into N discrete layers labeled as $n = 1, 2, 3, \ldots, N$, where $n = 1(N)$ is the top(bottom). The discrete form of equation (6) for the interior layers (i.e., $n \neq 1$ or N) of the slab is

$$\begin{aligned} L_\alpha = \frac{\mu^2}{\kappa^0_{\alpha n}} &\left\{ -\frac{1}{z_{n+1} - z_{n-1}} \left[\left(\frac{1}{\kappa^0_{\alpha n}} + \frac{1}{\kappa^0_{\alpha n+1}} \right) \left(\frac{\delta U_{\alpha n+1} - \delta U_{\alpha n}}{z_{n+1} - z_n} \right) - \left(\frac{1}{\kappa^0_{\alpha n}} + \frac{1}{\kappa_{\alpha n-1}} \right) \left(\frac{\delta U_{\alpha n} - \delta U_{\alpha n-1}}{z_n - z_{n-1}} \right) \right] \right\} \\ &+ \frac{\mu^2}{\kappa^{02}_{\alpha n}} \sum_{\alpha'} (E_{\alpha\alpha' n} \delta U_{\alpha' n}) \left\{ \frac{1}{z_{n+1} - z_{n-1}} \left[\left(\frac{1}{\kappa^0_{\alpha n}} + \frac{1}{\kappa^0_{\alpha n+1}} \right) \left(\frac{U^0_{\alpha n+1} - U^0_{\alpha n}}{z_{n+1} - z_n} \right) - \left(\frac{1}{\kappa^0_{\alpha n}} + \frac{1}{\kappa^0_{\alpha n-1}} \right) \left(\frac{U^0_{\alpha n} - U^0_{\alpha n-1}}{z_n - z_{n-1}} \right) \right] \right\} \\ &+ \frac{\mu^2}{\kappa^0_{\alpha n}} \left\{ \frac{1}{z_{n+1} - z_{n-1}} \left[\left(\frac{1}{\kappa^{02}_{\alpha n}} \sum_{\alpha'} E_{\alpha\alpha' n} \delta U_{\alpha' n} + \frac{1}{\kappa^{02}_{\alpha n+1}} \sum_{\alpha'} E_{\alpha\alpha' n+1} \delta U_{\alpha' n+1} \right) \left(\frac{U^0_{\alpha n+1} - U^0_{\alpha n}}{z_{n+1} - z_n} \right) \right. \right. \\ &\left. \left. - \left(\frac{1}{\kappa^{02}_{\alpha n}} \sum_{\alpha'} E_{\alpha\alpha' n} \delta U_{\alpha' n} + \frac{1}{\kappa^{02}_{\alpha n-1}} \sum_{\alpha'} E_{\alpha\alpha' n-1} \delta U_{\alpha' n-1} \right) \left(\frac{U^0_{\alpha n} - U^0_{\alpha n-1}}{z_n - z_{n-1}} \right) \right] \right\} \\ &+ \delta U_{\alpha n} - \frac{1}{\kappa^0_{\alpha n}} \sum_{\alpha'} F_{\alpha\alpha' n} \delta U_{\alpha' n} + \frac{Q^0_{\alpha n}}{\kappa^{02}_{\alpha n}} \sum_{\alpha'} E_{\alpha\alpha' n} \delta U_{\alpha' n} , \end{aligned} \tag{A3}$$

and equation (7) for L_α becomes

$$L_{\alpha n} = \frac{\mu^2}{\kappa^0_{\alpha n}} \left\{ \frac{1}{z_{n+1} - z_{n-1}} \left[\left(\frac{1}{\kappa^0_{\alpha n}} + \frac{1}{\kappa^0_{\alpha n+1}} \right) \left(\frac{U^0_{\alpha n+1} - U^0_{\alpha n}}{z_{n+1} - z_n} \right) - \left(\frac{1}{\kappa^0_{\alpha n}} + \frac{1}{\kappa^0_{\alpha n-1}} \right) \left(\frac{U^0_{\alpha n} - U^0_{\alpha n-1}}{z_n - z_{n-1}} \right) \right] \right\} - U^0_{\alpha n} + \frac{Q^0_{\alpha n}}{\kappa^0_{\alpha n}} . \tag{A4}$$

This may be written in a compact matrix equation form (see Mihalas 1978):

$$-\mathbf{A}_n \cdot \delta \boldsymbol{U}_{n-1} + \mathbf{B}_n \cdot \delta \boldsymbol{U}_n - \mathbf{C}_n \cdot \delta \boldsymbol{U}_{n+1} = \boldsymbol{L}_n , \tag{A5}$$

where $\delta \boldsymbol{U}$ and $\boldsymbol{L}$ are vectors of dimension α, and $\mathbf{A}_n$, $\mathbf{B}_n$, and $\mathbf{C}_n$ are square $\alpha \times \alpha$ matrices. In the standard linear case, $\mathbf{B}_n$ is a full matrix, while $\mathbf{A}_n$ and $\mathbf{C}_n$ are diagonal. Here all matrices are full.

To complete the set of equations, boundary conditions are required. At the top of the slab ($z = 0$, $n = 1$), the second-order boundary condition with no external illumination is

$$\begin{aligned} L_{\alpha 1} = &\frac{2\mu^2}{z_2^2 \kappa^{02}_{\alpha 1}} (\delta U_{\alpha 1} - \delta U_{\alpha 2}) + \frac{2\mu}{z_2 \kappa^0_{\alpha 1}} \delta U_{\alpha 1} + \frac{2\mu U^0_{\alpha 1}}{z_2 \kappa^{02}_{\alpha 1}} \sum_{\alpha'} E_{\alpha\alpha' 1} \delta U_{\alpha' 1} + \frac{\mu U^0_{\alpha 1}}{z_2 \kappa^{02}_{\alpha 1}} \left(\sum_{\alpha'} E_{\alpha\alpha' 2} \delta U_{\alpha' 2} - \sum_{\alpha'} E_{\alpha\alpha' 1} \delta U_{\alpha' 1} \right) \\ &+ \frac{\mu}{z_2 \kappa^{02}_{\alpha 1}} (\kappa^0_{\alpha 2} - \kappa^0_{\alpha 1}) \delta U_{\alpha 1} + \frac{2 U^0_{\alpha 1}}{\kappa^0_{\alpha 1}} \sum_{\alpha'} E_{\alpha\alpha' 1} \delta U_{\alpha' 1} + \delta U_{\alpha 1} - \frac{1}{\kappa^0_{\alpha 1}} \sum_{\alpha'} F_{\alpha\alpha' 1} \delta U_{\alpha' 1} - \frac{Q^0_{\alpha 1}}{\kappa^{02}_{\alpha 1}} \sum_{\alpha'} E_{\alpha\alpha' 1} \delta U_{\alpha' 1} , \end{aligned} \tag{A6}$$

where

$$L_{\alpha 1} = \frac{2\mu^2}{z_2^2 \kappa^{02}_{\alpha 1}} (U^0_{\alpha 2} - U^0_{\alpha 1}) - \frac{\mu U^0_{\alpha 1}}{z_2 \kappa^0_{\alpha 1}} - \frac{\mu U^0_{\alpha 1}}{z_2} \frac{\kappa^0_{\alpha 2}}{\kappa^{02}_{\alpha 1}} - U^0_{\alpha 1} + \frac{Q^0_{\alpha 1}}{\kappa^0_{\alpha 1}} . \tag{A7}$$

In standard Feautrier form, this takes the form

$$\mathbf{B}_1 \cdot \delta \boldsymbol{U}_1 - \mathbf{C}_1 \cdot \delta \boldsymbol{U}_2 = \boldsymbol{L}_1 . \tag{A8}$$

The boundary condition at the bottom of the slab ($z = z_N$, $n = N$) for complete reflection is

$$L_{\alpha N} = \frac{2\mu^2}{\kappa^{02}_{\alpha N}} \left(\frac{1}{z_{N-1} - z_N} \right)^2 (\delta U_{\alpha N} - \delta U_{\alpha N-1}) + \frac{2 U^0_{\alpha N}}{\kappa^0_{\alpha N}} \sum_{\alpha'} E_{\alpha\alpha' N} \delta U_{\alpha' N} + \delta U_{\alpha N} - \frac{1}{\kappa^0_{\alpha N}} \sum_{\alpha'} F_{\alpha\alpha' N} \delta U_{\alpha' N} - \frac{Q^0_{\alpha N}}{\kappa^{02}_{\alpha N}} \sum_{\alpha'} E_{\alpha\alpha' N} \delta U_{\alpha' N} , \tag{A9}$$

where

$$L_{\alpha N} = \frac{2\mu^2}{\kappa^{02}_{\alpha N}} \left(\frac{1}{z_{N-1} - z_N} \right)^2 (U^0_{\alpha N-1} - U^0_{\alpha N}) - U^0_{\alpha N} + \frac{Q^0_{\alpha N}}{\kappa^0_{\alpha N}} . \tag{A10}$$

This can also be written in standard Feautrier form

$$-\mathbf{A}_N \cdot \delta \boldsymbol{U}_{N-1} + \mathbf{B}_N \cdot \delta \boldsymbol{U}_N = \boldsymbol{L}_N . \tag{A11}$$

Equations (A5), (A8), and (A11) represent a closed set of coupled linear equations for the perturbation in the photon density. Given a starting solution, the set can be solved by standard numerical techniques and then iterated until convergence.

REFERENCES

Alexander, S. G., Mészáros, P., and Bussard, R. W. 1989, in preparation.
Bussard, R. W. 1980, *Ap. J.*, **237**, 970.
Bussard, R. W., Alexander, S., and Mészáros, P. 1986, *Phys. Rev. D*, **34**, 440.
Daugherty, J. K., and Harding, A. K. 1987, *Ap. J.*, **309**, 362.
Gnedin, Yu. N., Pavlov, G. G., and Shibanov, Yu. A. 1978, *Soviet Phys.—JETP (Letters)*, **27**, 305.
Harding, A. K., Mészáros, P., Kirk, J. G., and Galloway, D. J. 1984, *Ap. J.*, **278**, 369.

Kaminker, A. D., Pavlov, G. G., and Shibanov, Yu. A. 1982, *Ap. Space Sci.*, **86**, 249.
———. 1983, *Ap. Space Sci.*, **91**, 167.
Kirk, J. G., and Melrose, D. B. 1986, *Astr. Ap.*, **156**, 277.
Melrose, D. B., and Kirk, J. G. 1986, *Astr. Ap.*, **156**, 268.
Mészáros, P., and Nagel, W. 1985*a*, *Ap. J.*, **298**, 147.
———. 1985*b*, *Ap. J.*, **299**, 138.
Mészáros, P., Pavlov, G. G., and Shibanov, Yu. A. 1989, *Ap. J.*, **337**, 426.
Mészáros, P., and Ventura, J. 1978, *Phys. Rev. Letters*, **41**, 1544.
———. 1979, *Phys. Rev. D*, **19**, 3565.
Mihalas, D. 1978, *Stellar Atmospheres* (San Francisco: Freeman).
Nagel, W. 1981*a*, *Ap. J.*, **251**, 278.
———. 1981*b*, *Ap. J.*, **251**, 288.
———. 1982, in *Accreting Neutron Stars*, ed. W. Brinkmann and J. Truemper (MPE Rept. 177), p. 302.
Pavlov, G. G., and Shibanov, Yu. A. 1979, *Soviet Phys.—JETP Letters*, **49**, 741.
Pavlov, G. G., Shibanov, Yu. A., and Yakovlev, D. G. 1980, *Ap. Space Sci.*, **73**, 33.
Ventura, J., Nagel, W., and Mészáros, P. 1979, *Ap. J. (Letters)*, **233**, L125.
Voges, W., Pietsch, W., Reppin, C., Trümper, J., Kendziorra, E., and Staubert, R. 1982, *Ap. J.*, **263**, 803.

S. G. Alexander: Physics Department, 104 Davey Laboratory, Pennsylvania State University, University Park, PA 16802

R. W. Bussard: Space Science Laboratory, NASA Marshall Space Flight Center, Huntsville, AL 35812

P. Mészáros: Astronomy Department, 525 Davey Laboratory, Pennsylvania State University, University Park, PA 16802